

## Measurements of ice water content in tropopause region Arctic cirrus during the SAGE III Ozone Loss and Validation Experiment (SOLVE)

A. Gannet Hallar,<sup>1,2</sup> Linnea M. Avallone<sup>1,3</sup> Robert L. Herman,<sup>4</sup> Bruce E. Anderson,<sup>5</sup>  
and Andrew J. Heymsfield<sup>6</sup>

Received 13 November 2003; revised 7 June 2004; accepted 18 June 2004; published 8 September 2004.

[1] A new instrument, the closed-path laser hygrometer (CLH), was flown on the NASA DC-8 aircraft during the Stratospheric Aerosol and Gas Experiment (SAGE) III Ozone Loss and Validation Experiment (SOLVE) campaign in 1999–2000 to measure condensed-phase water. The ice water content (IWC) of Arctic cirrus was determined from in situ measurements of condensed- and gas-phase water. The IWC values obtained from the CLH observations are compared to those determined by integrating particle size distributions measured by a Forward Scattering Spectrometer Probe (FSSP) also flown on the DC-8. The considerably greater IWC seen by the CLH implies the presence of particles with diameters greater than the FSSP's upper limit of 20  $\mu\text{m}$ . The evidence for and implications of the presence of large ice crystals in Arctic cirrus is discussed. *INDEX TERMS*: 0320 Atmospheric Composition and Structure: Cloud physics and chemistry; 0365 Atmospheric Composition and Structure: Troposphere—composition and chemistry; 0394 Atmospheric Composition and Structure: Instruments and techniques; *KEYWORDS*: ice water content, cirrus, heterogeneous chemistry

**Citation:** Hallar, A. G., L. M. Avallone, R. L. Herman, B. E. Anderson, and A. J. Heymsfield (2004), Measurements of ice water content in tropopause region Arctic cirrus during the SAGE III Ozone Loss and Validation Experiment (SOLVE), *J. Geophys. Res.*, 109, D17203, doi:10.1029/2003JD004348.

### 1. Introduction

[2] Cirrus clouds are one of the most commonly occurring cloud types [Wylie *et al.*, 1994; Wylie and Menzel, 1999], with an extensive range of macrophysical [Dowling and Radke, 1990] and microphysical [Ström and Heintzenberg, 1994] properties that make modeling them a challenge. Yet, understanding the interaction of clouds with solar and terrestrial radiation represents one of the greatest uncertainties in the prediction of future global climate [Intergovernmental Panel on Climate Change, 2001]. Cirrus clouds are of special interest in this regard because of their location in the upper troposphere, where their unique optical and microphysical properties contribute to local radiative heating. For example, relatively small changes in the particle size distributions within cirrus clouds can alter significantly the modeled optical depth [Kinne and Liou, 1989]. Lohmann and Roeckner [1995] further showed that climate sensitivity can change by as much as 40% when the properties of cirrus

range from transparent to opaque limits. Therefore accurate knowledge of cirrus cloud properties, including particle size distributions and ice water content, is essential to improving climate predictions based on models that include parameterizations of cirrus clouds [Sun and Rikus, 1999].

[3] The thin, cold, often subvisual cirrus found near the tropical tropopause have been shown to exert significant radiative forcing (1.2–1.7  $\text{W m}^{-2}$ ); however, relatively few in situ measurements of their microphysical properties have been reported [Heymsfield, 1986; McFarquhar *et al.*, 2000; Thomas *et al.*, 2002; Peter *et al.*, 2003]. Indeed, there is a paucity of in situ cirrus cloud sampling near the tropopause in all geographical regions, due in part to the difficulty of reaching these altitudes with the appropriate instrumentation. Until very recently, only three relatively comprehensive studies of tropopause cirrus have been performed; these comprise measurements from the WB-57F made near the Marshall Islands in the mid 1970s [Heymsfield and Jahnsen, 1974; Heymsfield, 1986], from the Aeromet LearJet in the same location in the early 1980s [Booker and Stickel, 1982], and from the Deutsche Zentrum für Luft- und Raumfahrt (DLR) Falcon over the Arctic during Polar Stratospheric Aerosol Experiment (POLSTAR) 1997 [Schiller *et al.*, 1999]. Results from the NASA Cirrus Regional Study of Tropical Anvils and Cirrus Layers–Florida Area Cirrus Experiment (CRYSTAL-FACE) mission (summer 2002) will contribute a great deal of information regarding particle size distributions, ice water content, and chemical composition of cirrus in the subtropics [Jensen *et al.*, 2004].

<sup>1</sup>Program in Atmospheric and Oceanic Sciences, University of Colorado, Boulder, Colorado, USA.

<sup>2</sup>Now at NASA Ames Research Center, Moffett Field, California, USA.

<sup>3</sup>Laboratory for Atmospheric and Space Physics, University of Colorado, Boulder, Colorado, USA.

<sup>4</sup>Jet Propulsion Laboratory, California Institute of Technology, Pasadena, California, USA.

<sup>5</sup>NASA Langley Research Center, Hampton, Virginia, USA.

<sup>6</sup>National Center for Atmospheric Research, Boulder, Colorado, USA.

[4] One conclusion reached from these studies is that mean particle size and dominant crystal habit can be generally related to ambient temperature, with mean particle size decreasing as temperature decreases. The work of *Heymsfield and Platt* [1984] summarizes these results and still serves as the basis for parameterizations in many cloud models. Of particular interest is the presence of some large crystals (with maximum dimension,  $d$ ,  $> 20 \mu\text{m}$ ) with unique individual structures that interact differently with radiation. At temperatures below  $-50^\circ\text{C}$ , in cirrus that form in situ rather than from convection, crystal shapes are predominately hollow or solid columns, although occasionally some hexagonal plates and thick plates are seen near cloud tops. As opposed to warmer temperatures ( $-20^\circ\text{C}$  to  $-40^\circ\text{C}$ ) at which polycrystalline shapes can form, single crystals predominate at temperatures below  $-50^\circ\text{C}$  [*Heymsfield and Platt*, 1984]. Further, the variety of shapes, which are typically unresolved by particle sizing instruments, and their low densities (compared to spherical particles of the same diameter) can lead to significant errors in determining the cloud ice water content (IWC). IWC is an important standard parameter for calculating the radiative properties of cirrus clouds [*Sun and Rikus*, 1999].

[5] In addition to their role in the global energy balance, cirrus clouds may be important players in tropopause region ozone trends. An analysis of ozonesonde observations by *Logan et al.* [1999] showed a significant decrease in stratospheric ozone at all stations in the middle and high latitudes of the Northern Hemisphere, with largest ozone losses in the late winter/early spring lowermost stratosphere. One explanation for the observed trend is local chemical loss. *Borrmann et al.* [1996] suggested that heterogeneous conversion of reservoir chlorine to reactive forms could take place on cirrus cloud particles. Reactive chlorine would then participate in catalytic ozone destruction chemistry. Although evidence to support this mechanism is still contradictory [see *Smith et al.*, 2001; *Thornton et al.*, 2003; *Bregman et al.*, 2002], the size of cirrus particles would play a crucial role in determining the rate at which chlorine activation could take place. For a given ice water content, the total surface area in a cloud is a sensitive function of the size distribution of the particles; more smaller particles will have a larger surface area than a few larger ones.

[6] Cirrus clouds may also affect the reactive nitrogen budget in the tropopause region. For example, models tend to overestimate the  $\text{HNO}_3/\text{NO}_x$  ratio in the upper troposphere in most geographical locations [*Singh et al.*, 1994; *Fan et al.*, 1994]. One possible solution to this discrepancy is the uptake of  $\text{HNO}_3$  onto the surface of cirrus cloud particles in the upper troposphere, which can lead to irreversible removal of  $\text{HNO}_3$ . Significant uptake of  $\text{HNO}_3$  by water ice at temperatures characteristic of the tropopause region has been demonstrated in laboratory studies [*Abbatt*, 1997; *Zondlo et al.*, 1997] as well as by field measurements [*Weinheimer et al.*, 1998; *Feigl et al.*, 1999; *Hervig and McHugh*, 2002; *Kondo et al.*, 2003]. The fractional surface area coverage of  $\text{HNO}_3$  on ice is a function of temperature [*Hynes et al.*, 2002], reaching as much as a monolayer below 200 K [*Zondlo et al.*, 2000; *Abbatt*, 1997]. Large particles provide significant surface area and also, if large enough, may compete effectively to irreversibly remove  $\text{HNO}_3$  via sedimentation [*Lawrence*

and *Crutzen*, 1998]. Thus an accurate determination of the particle size distributions within cirrus is essential for understanding the chemistry of  $\text{HNO}_3$  in the upper troposphere.

[7] In this paper we present measurements of the ice water content of Arctic tropopause region cirrus clouds made from the NASA DC-8 during the Stratospheric Aerosol and Gas Experiment (SAGE) III Ozone Loss and Validation Experiment (SOLVE) campaign of 1999–2000. By comparing these observations to IWC calculated from simultaneous measurements of particle size distributions, we provide strong evidence for the unexpected presence of large ice crystals ( $d \approx 100 \mu\text{m}$ ) in these cold ( $199 \text{ K} < T < 210 \text{ K}$ ) clouds.

## 2. Experiment

[8] The SOLVE campaign was based in Kiruna, Sweden, during the winter of 1999–2000; its main goal was learning more about the causes of ozone loss in the Arctic lower stratosphere [*Newman et al.*, 2002]. Observations from three instruments based on the DC-8 are discussed in this paper; a brief description of each is given below.

### 2.1. Forward Scattering Spectrometer Probe-300

[9] The Forward Scattering Spectrometer Probe (FSSP-300), built by Particle Measurements Systems (Boulder, Colorado), was originally developed for the study of stratospheric aerosol and polar stratospheric cloud particles. It is now widely used in aerosol physics and tropospheric chemistry [*Baumgardner et al.*, 1992]. The FSSP samples particles in the free stream so that they are not altered in size or shape by an inlet system. Individual particles are detected and their size is determined on the basis of the intensity of light that they scatter as they pass through the focused beam of a helium-neon laser. The size of the particle is determined using Mie theory, assuming that the particles are spherical with a known refractive index. During SOLVE, the FSSP-300's 31 size bins were configured to cover the size range 0.4 to  $20 \mu\text{m}$ . A refractive index of 1.57, appropriate for sulfuric acid aerosols, was assumed throughout.

[10] Uncertainties in the FSSP-300 measurement fall into two categories: concentration uncertainties and sizing errors, which both propagate through to the calculation of total condensed material. Concentration uncertainties typically are about 25%, while the various contributions to sizing errors amount to approximately 60% uncertainty in mass concentration [*Baumgardner et al.*, 1992]. The asphericity of ice particles adds a further complication (see section 3), as does the potential for large ice crystals to shatter on the FSSP inlet [*Gardiner and Hallet*, 1985], although recent studies suggest that this causes overestimation of number concentration by about a factor of two or less [*Field et al.*, 2003].

### 2.2. Hygrometers

[11] The development of the tunable diode laser (TDL) for measurements of stratospheric and upper tropospheric water began in 1992 at the Jet Propulsion Laboratory (JPL) [*May*, 1998]. The original instrument was designed with an open, external absorption path to avoid contamination problems typical of internal sample cells. This instrument and others similar to it have flown on several aircraft

platforms, including the NASA ER-2, DC-8, and WB-57F, and the NCAR C-130. A complete description of the JPL TDL hygrometer (hereinafter JLH) is provided by May [1998]. The University of Colorado closed-path laser hygrometer (CLH) is virtually identical to the JLH, except that it has an internal absorption cell and is optimized for detecting the larger abundances of water typical of the troposphere. The salient details of the instruments are given below, and any differences between the JLH and CLH are noted.

[12] Both the open and closed-path hygrometers use low-power, near-infrared ( $\sim 1.37 \mu\text{m}$ ,  $7306.7518 \text{ cm}^{-1}$  for CLH) laser sources developed and manufactured by the JPL Microdevices Laboratory. These lasers are favored because they can operate near room temperature, eliminating the need for cryogenic cooling. The JLH optical path is a simple “there-and-back” design, with a total path length of 50 cm, providing a detection limit of about 5 ppm. The CLH has a single-pass absorption cell with a length of 27.6 cm. This cell consists of a 6 mm ID stainless steel tube sealed at both ends with antireflection-coated quartz windows. This short path length limits the detection of water to values greater than about 10 ppm for a 1-s integration. The flow rate through the CLH was fixed by a mass flow controller (Tylan FC2901, Millipore, Inc.) set at approximately 1.8 standard L  $\text{min}^{-1}$ . The flow path was heated to  $40^\circ\text{C}$  ( $\pm 0.1^\circ\text{C}$ ) to prevent condensation of water during transition through regions of varying ambient temperatures and humidities. The heat also helped to evaporate ice crystals and water droplets, a process accomplished primarily by ram heating at the inlet. Heat transfer calculations show that particles with  $d \leq 100 \mu\text{m}$  are completely evaporated by the combination of ram and direct heating.

[13] Water data in both the CLH and JLH instruments are obtained by scanning the laser frequency repetitively across a small wavelength range ( $1\text{--}2 \text{ cm}^{-1}$ ) containing the spectral feature of interest. Direct and second-harmonic (2f) absorption spectra are obtained every 128 ms. The laser control, signal processing, and data acquisition are accomplished with custom circuit boards (MayComm, Inc., Pasadena, California). Water vapor mixing ratios are calculated on the basis of the observed signal strength and a processing matrix relating signal strength to mixing ratio as a function of temperature and pressure. This matrix is generated from laboratory calibration data and knowledge of the spectroscopic parameters for the absorption feature.

[14] Data from the TDL spectrometers generally have precisions of 1–2% for an integration time of 1 s. Accuracy is dependent on laboratory calibrations, which are accomplished using either a water vapor measurement standard, such as a NIST-traceable chilled mirror hygrometer, or a dew point generator such as the LiCor LI-610. For this study, the JLH was calibrated relative to a NIST-traceable General Eastern chilled mirror hygrometer (GE 1311DR). The CLH was calibrated relative to a LiCor LI-610, using a dynamic dilution system consisting of several MKS model 640 flow controllers. The resulting accuracy of water mixing ratios from each instrument is about  $\pm 15\%$  ( $2\sigma$ ).

[15] During SOLVE, the CLH measured behind a heated, forward facing inlet located on the second portside window plate of the DC-8. The inlet is subisokinetic, with a sample flow velocity of approximately  $4.5 \text{ m s}^{-1}$  compared to a

typical aircraft speed of  $230 \text{ m s}^{-1}$ . This condition results in inertially enhanced particle sampling. Although the inlet is slightly anisoaxial, with an angle of approximately  $4^\circ$  between the direction of the free stream and the sample inlet, all calculations below assume isoaxial flow for simplicity. Errors resulting from this simplification are believed to be small.

[16] For an upper limit estimate of the particle enhancement efficiency, the ratio of the aircraft speed and inlet intake speed was calculated [Belyaev and Levin, 1972; Fahey et al., 1989; Feigl et al., 1999]. The intake speed was calculated from the known volume intake of the instrument at standard temperature and pressure, along with the ambient pressure, ambient temperature, and true air speed of the aircraft. Ram heating created by adiabatic compression at the inlet was also taken into account [Schlichting, 1979]. The enhancement factor, which varies with aircraft speed, ambient temperature, and ambient pressure, averaged about 65 and ranged from 40 to 120 over the course of a flight.

[17] The simple velocity ratio calculation described above ignores the effect of particle size on the extent of inertial enhancement. A more accurate estimate of the enhancement factor was obtained from a fluid dynamical calculation of flow in and around the inlet, using a model of the streamlines around the DC-8 fuselage. These calculations were carried out with the computational fluid dynamics package FLUENT (FLUENT, Inc., Lebanon, New Hampshire) by D. Gesler of the University of Denver. A similar calculation had previously been done for the University of Denver particle instrument inlet, which was located approximately 0.6 m in front of the CLH inlet. The CLH inlet was assumed to be isoaxial and the particles were modeled as perfect spheres. The results of this calculation for one set of conditions are shown in Figure 1. Given the similarity of the results obtained from the fluid dynamical calculation and the ratio-of-velocities calculation, we have used the latter method to calculate the inlet enhancement efficiency on a 1-s time basis throughout the flights analyzed here.

[18] Size-resolved particulate water measurements were not available on this mission, so a size-independent enhancement efficiency was used to convert the “total” water measured by the CLH to ambient water mass. This assumption results in very little error. Using a size distribution calculated from the FSSP observations and the size-dependent enhancement efficiency from the FLUENT model, we estimate that particles smaller than  $4 \mu\text{m}$  contribute about 2–3% to the total mass of water sampled by the CLH.

### 3. Analysis Method

[19] One of the main goals of the analysis presented here is to compare the mass of particulate water measured by the laser hygrometer with that deduced from the FSSP size distribution. The first step in this process was to remove the water vapor from the total water measurement, leaving a quantity that is due only to condensed-phase water.

[20] After time offsets between the JLH and CLH were accounted for, distinct similar features appeared in the two data sets. Trend analyses were used to account for differences between the baselines of the JLH and CLH data.

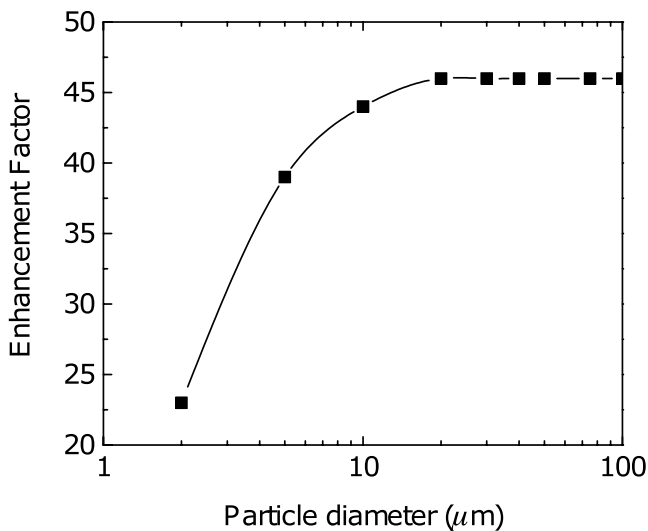


**Figure 1.** Particle enhancement factor as a function of particle diameter ( $\mu\text{m}$ ) calculated using the FLUENT fluid dynamics code.

Primarily these differences are due to the lower sensitivity (i.e., larger detection limit) of the CLH, but pressure dependences in the instrument calibrations and variations in the dryness of the instrument optics also contribute. Once the drifts in baseline were accounted for, the CLH and JLH data agreed to within  $\pm 2$  ppm during all cloudless periods. An example is shown in Figure 2.

[21] Next, the JLH data were subtracted from the baseline-corrected CLH data. By subtracting the water vapor, only signal due to evaporated cirrus particles remained, including the enhancement created by the subsokinetic inlet. The enhancement factor was calculated as described above, and the CLH data were divided by it to obtain the ambient mixing ratio of particulate water. This quantity was converted to particulate water mass using the measurements of ambient temperature and pressure made by the DC-8 meteorological sensor package.

[22] The FSSP particle volume data, which are derived from the measured number and size distributions, were converted to water mixing ratio using the ambient pressure and temperature, and assuming spherical ice particles with a density of  $0.8 \text{ g cm}^{-3}$ . This density was chosen based on observations of cirrus crystal habits at temperatures similar to those encountered during SOLVE. Although these habit measurements were made in the midlatitudes, they are the only such observations available. Unpublished data [Heymsfield, 1986] show that, at temperatures around 200 K, cirrus cloud particles are an approximately equal allotment of trigonal plates and columns. Although the smaller column crystals tend to be solid ice, the larger columns have hollow regions. Assuming that the average ice crystal shape is a column with a width-to-length ratio of 0.4, a density of  $0.8 \text{ g cm}^{-3}$  gives the best representation of the water content of the bulk condensed phase.

[23] Despite evidence to the contrary, we have assumed that all particles encountered were spherical in the analysis presented here. The primary reason for this is that the FSSP algorithm assumes spherical particles. Since the FSSP does not measure particle orientation, when a columnar particle is

sampled, the reported diameter depends upon the particle's orientation within the beam of the laser. It should be noted that the assumption of spherical particles results in the maximum possible quantity of condensed water for a given diameter based on the FSSP size distributions. If the calculations were performed assuming columnar particles instead of spherical ones, the condensed water calculated from the FSSP observations would be lower by about a factor of 4.

#### 4. Results

[24] Cirrus clouds were encountered by the DC-8 aircraft several times during the SOLVE mission. In this study, data from five flights were analyzed; details of these cloud encounters are given in Table 1. Ambient temperatures during these periods were between 199 K and 212 K, at altitudes ranging from 10.5 to 12.5 km. As shown in column 4 of Table 1, these cloud encounters were all within about 1.5 km of the tropopause, as determined by the Microwave Temperature Profiler (MTP) onboard the DC-8. The MTP algorithm uses the World Meteorological Organization definition of the tropopause, the lowest altitude at which the lapse rate,  $dT/dz$ , is less than  $-2 \text{ K km}^{-1}$  [Roe and Jasperson, 1980]. It should be noted that this definition can mislocate the tropopause in regions where the temperature gradient is relatively flat with altitude, such as within the polar vortex (M. J. Mahoney, personal communication, 2002).

[25] An example of particulate water data calculated from observations made during a typical cirrus cloud encounter (on 25 January 2000) is shown in Figure 3. It is readily apparent that the particulate water observed by the CLH is considerably greater than that calculated from the FSSP particle data. In general the features seen in the FSSP data and the CLH observations were similar, indicating that both are responding to cloud particles. However, the CLH always observed more particulate water than that calculated from the coincident FSSP particle data.

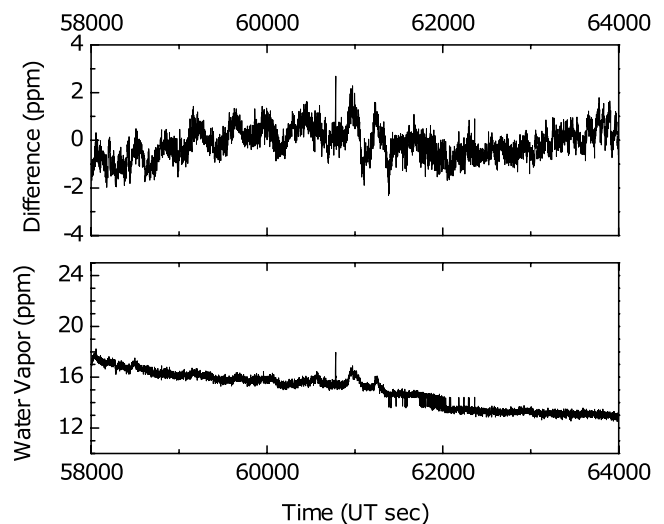


**Figure 2.** (top) Difference between Jet Propulsion Laboratory tunable diode laser hygrometer (JLH) and baseline-adjusted closed-path laser hygrometer (CLH) data. (bottom) JLH water measurements during a clear-sky period.

**Table 1.** Cloud Encounter Details

Cloud Periods	Time, UT s	Altitude, km	$\Delta Z$ , <sup>a</sup> km	Temperature, K	IWC, $\text{g m}^{-3}$
23 January 2000, 1	33025–35168	$10.67 \pm 0.01$	$-0.83 \pm 0.04$	$205.3 \pm 0.2$	$1.65 \times 10^{-3}$
23 January 2000, 2	43547–44527	$11.42 \pm 0.25$	$-0.10 \pm 0.26$	$201.4 \pm 0.5$	$6.55 \times 10^{-4}$
23 January 2000, 3	48217–50166	$11.89 \pm 0.01$	$-0.20 \pm 0.17$	$203.1 \pm 0.1$	$1.41 \times 10^{-3}$
23 January 2000, 4	51056–58878	$12.39 \pm 0.24$	$-0.43 \pm 0.28$	$200.5 \pm 1.7$	$1.48 \times 10^{-3}$
25 January 2000, 1	35373–35846	$10.67 \pm 0.00$	$0.04 \pm 0.07$	$208.6 \pm 0.4$	$2.31 \times 10^{-3}$
25 January 2000, 2	36139–40800	$11.28 \pm 0.01$	$-0.98 \pm 0.39$	$207.7 \pm 0.6$	$4.77 \times 10^{-4}$
25 January 2000, 3	41629–45116	$11.41 \pm 0.25$	$-1.02 \pm 0.37$	$206.8 \pm 1.7$	$5.55 \times 10^{-4}$
25 January 2000, 4	48710–50905	$11.89 \pm 0.01$	$-0.42 \pm 0.37$	$203.4 \pm 0.7$	$7.01 \times 10^{-4}$
8 March 2000, 1	37967–54370	$10.87 \pm 0.39$	$-0.81 \pm 0.35$	$206.8 \pm 3.1$	$1.39 \times 10^{-3}$
9 March 2000, 1	66084–67204	$10.78 \pm 0.23$	$0.02 \pm 0.27$	$211.3 \pm 0.7$	$1.39 \times 10^{-3}$
9 March 2000, 2	73509–76527	$11.71 \pm 0.31$	$0.00 \pm 0.20$	$204.6 \pm 1.4$	$2.70 \times 10^{-3}$
11 March 2000, 1	49161–55188	$11.57 \pm 0.41$	$0.15 \pm 0.52$	$201.0 \pm 1.7$	$1.20 \times 10^{-3}$

<sup>a</sup>Distance from tropopause.

[26] Could these discrepancies be due to instrumental errors? The accuracy of the CLH measurement is well established and the corresponding uncertainty is not sufficiently large to account for the difference between the observed and calculated particulate water abundances. In addition, we are using an upper limit estimate of the inlet enhancement factor. A smaller enhancement factor would result in greater particulate water amounts from the CLH observations and would only make the discrepancy greater.

[27] Errors in the FSSP observations could also contribute to the difference between the observed and calculated particulate water amounts. The FSSP has an uncertainty in diameter of about  $\pm 30\%$ , which leads to an uncertainty in particle volume of  $\pm 90\%$ . The average particulate water concentrations for each cloud encounter as determined by the CLH and by the FSSP are shown in Figure 4 with error bars representing their respective accuracies. In no case do these error bars overlap the 1:1 correlation line. Although most points encompass the 1:10 correlation line within their errorbars, there is no consistent “offset” between the two data sets. The scatter of the points in Figure 4 makes this clear.

[28] The FSSP data were analyzed assuming that the particles were liquid sulfate aerosols, with a refractive index of  $1.57 + 0.0i$ . This refractive index is quite different from that of ice ( $m \approx 1.31$ ). If the appropriate refractive index for ice were used, the FSSP-300 as configured during SOLVE would have been sensitive to cirrus cloud particles in the size range of  $0.3\text{--}14\ \mu\text{m}$ , rather than  $0.4\text{--}20\ \mu\text{m}$ , as reported (D. Baumgardner, personal communication, 2001). If the measured particle size distribution were shifted toward the more appropriate smaller diameters, the gap between the FSSP particulate water and that calculated from the CLH observations would increase.

[29] The systematic uncertainties in the CLH and FSSP measurements discussed above represent a lower bound and an upper bound, respectively, to the particulate water abundances calculated from the two data sets. Thus the differences shown in Figure 4 are a lower limit to the discrepancy between the two determinations of particulate water. We also note that the differences between the CLH and the FSSP particulate water abundances do not appear to be related to temperature or altitude. As a result of all of this evidence, we believe that the discrepancies discussed here

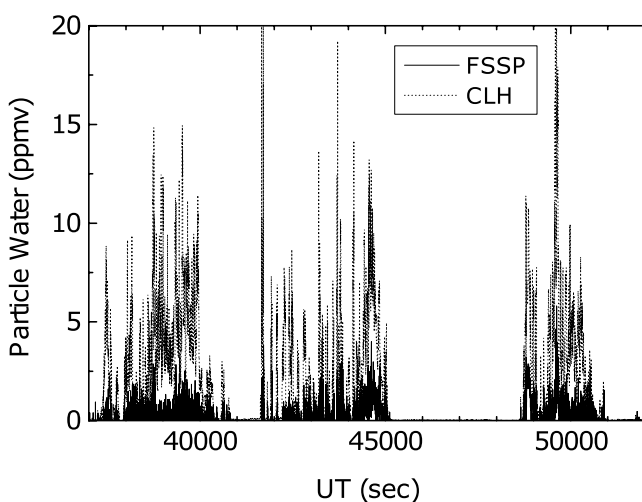


**Figure 3.** An example of the comparison of ice water content calculated from the CLH observations of particulate water (dashed line) and from the Forward Scattering Spectrometer Probe (FSSP) measurements of particle size distribution (solid line). Data are from the SOLVE flight on 25 January 2000.

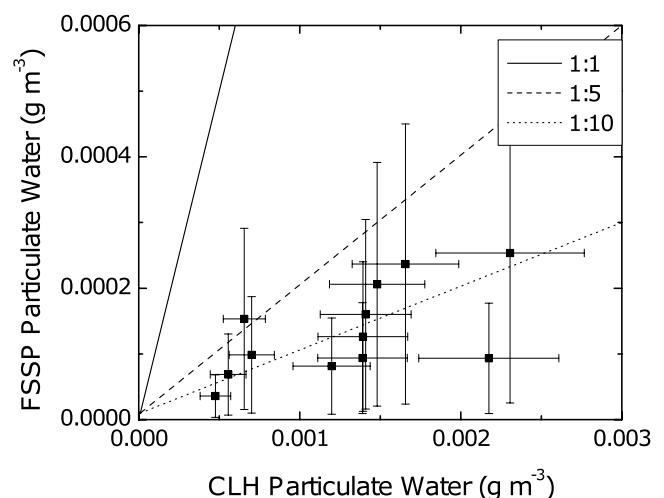


**Figure 4.** Scatterplot of the average ice water content (IWC) calculated from the CLH and from the FSSP for all cirrus encounters during SOLVE. Error bars represent  $2\sigma$  accuracy on each measurement. The lines show various ratios of the FSSP IWC to the CLH IWC.

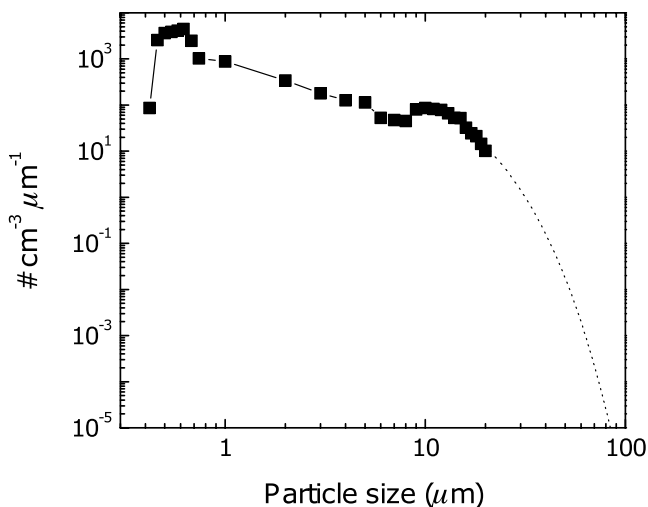


**Figure 5.** Example of a particle size distribution observed during the SOLVE campaign. The dashed line segment illustrates an extension of the size distribution in a lognormal fashion on the basis of the slope between 10 and 20  $\mu\text{m}$ . The measured size distribution is indicated by squares and the solid line.

are due to real differences in the range of particle sizes sampled by the two techniques.

## 5. Discussion

[30] One possible explanation for the differences between the FSSP and CLH particulate water abundances is the presence of cloud particles with diameters greater than the FSSP's upper limit of 20  $\mu\text{m}$ . In general, ice crystal sizes and concentrations primarily depend on temperature, with larger mean diameters present at warmer temperatures [Heymsfield and Platt, 1984]. Cirrus cloud particles have been measured in a variety of meteorological conditions, mostly within the temperature range of 215–250 K. However, those observations were made at midlatitudes or in the tropics, where cloud formation mechanisms, and hence the particle size distributions, may be different from those in the high latitudes. There is only one published study in which measurements of cirrus particles were made at temperatures around 200 K in the polar region [Meilinger *et al.*, 1999]. Unfortunately, the instrumentation on the POLSTAR 1997 campaign provided particle size distributions only between 0.15 and 10  $\mu\text{m}$  [Schiller *et al.*, 1999]. Goodman *et al.* [1989] found an occasional rare particle with maximum dimension greater than 100  $\mu\text{m}$  during impactor sampling of particles in the Antarctic stratosphere. However, it is not known if these particles were found in cirrus clouds or polar stratospheric clouds.

[31] Given the lack of appropriate comparisons for our study, we are forced to turn to particle size measurements made at similar temperatures in tropical and midlatitude regions at much higher altitudes [e.g., Heymsfield, 1986]. Heymsfield's 1986 study had minimum temperatures around 190–191 K, with corresponding particle sizes between 5 and 50  $\mu\text{m}$  (the minimum and maximum detection limits of the instrument). L. M. Miloshevich and A. J. Heymsfield (unpublished data, 1991) collected and pre-

served ice crystals and cloud droplets using the Formvar replication technique on a balloon platform during the First International Satellite Cloud Climatology Project (ISCCP) Regional Experiment (FIRE) II cirrus field campaign at midlatitudes [Miloshevich and Heymsfield, 1997]. They reported particle diameters between approximately 10 and 300  $\mu\text{m}$  within the temperature range of 208–218 K. Thus there is some evidence for the existence of particles larger than 20  $\mu\text{m}$  at temperatures similar to those encountered during the SOLVE cirrus penetrations.

[32] To see whether including larger particles improves the agreement between the FSSP and CLH particulate water abundances, we extended the FSSP size distributions in a lognormal fashion to diameters of 100  $\mu\text{m}$ , an upper limit consistent with previous observations in cold cirrus clouds. The slope of the distribution was determined on the basis of the slope of the observed size spectrum between 10 and 20  $\mu\text{m}$ . An example is shown in Figure 5. Such composite size distributions were created by averaging all 1-s measurements within a given cloud encounter. As illustrated by the time values in column 2 of Table 1, these averages range from 500 to 7500 s in length. Averaging large amounts of data in this manner minimizes errors from counting statistics in the large-particle channels. In most clouds (11 out of 12), the expanded lognormal size distribution did not account for all of the excess water seen by the CLH. Extending the FSSP size spectrum to 100  $\mu\text{m}$  represented, on average, 63% of the particulate water, varying between 30 and 145%.

[33] The need for more particulate mass beyond that provided by the lognormal distribution suggests that there may be one or more additional modes at larger sizes. Figure 6 shows a mass distribution based on the observations of midlatitude cirrus particles described above (L. M. Miloshevich and A. J. Heymsfield, unpublished data, 1991). An average mass distribution for the Arctic cirrus based on the FSSP observations from SOLVE is also shown. Although the quantity of water and the diameter at which the maximum amount of water was measured differ, a dominant

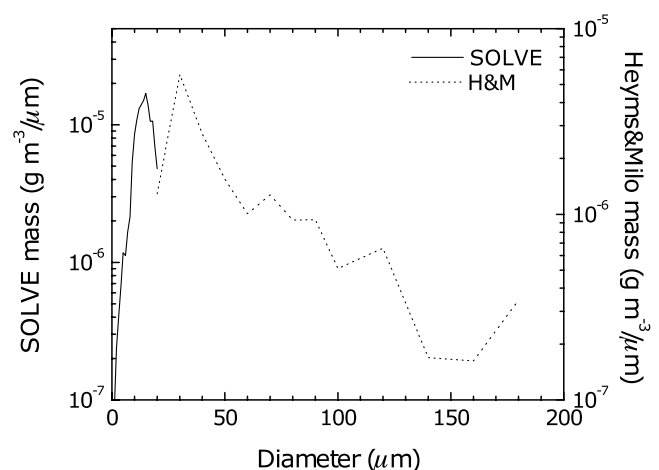


**Figure 6.** Mass distribution of particles in a midlatitude cirrus cloud at a temperature of 210 K (dashed line). Data are courtesy of A. J. Heymsfield and L. M. Miloshevich. Average mass distribution of particles in three different Arctic cirrus clouds sampled during the SOLVE campaign are shown (solid line).

mode is present at diameters between 10 and 30  $\mu\text{m}$  in both situations. As a result of the size limitations of the instrumentation used in these studies, the smaller (in the case of Miloshevich and Heymsfield) and larger (in this work) particles are not accounted for in these mass distributions.

[34] The presence of small but distinct modes at larger diameters in the Miloshevich and Heymsfield data give us cause to speculate that such features may also be present in Arctic cirrus, and that they might account for the “missing” particulate water. If the Miloshevich and Heymsfield distribution is shifted to smaller diameters and scaled so that the peak at small diameters matches that seen in the SOLVE data, we can estimate the additional mass that might be present in the modes at larger diameters. For the case shown in Figure 6, this procedure results in a factor-of-2 increase in mass over that given by the FSSP data alone. This is a significant improvement, although the value remains considerably lower than that measured by the CLH. However, given the large uncertainty in the actual shape of the particle size distribution at diameters greater than 20  $\mu\text{m}$ , this discrepancy is not worrisome.

[35] The potential presence of large particles in Arctic cirrus clouds is significant. Since particle fall speeds are proportional to the square of particle radius (assuming Stokes regime), these larger particles will fall considerably faster than smaller ones. For example, a 100  $\mu\text{m}$  particle falls about 100 times faster than a 10  $\mu\text{m}$  particle under the same atmospheric conditions. This means that larger particles can remove more mass from a region than small ones. The sedimentation of large particles in Type II (ice) polar stratospheric clouds is well known to be the main mechanism for dehydration of the winter polar vortex. It is possible that the large particles we infer here to be present in Arctic cirrus clouds are also actively redistributing water vapor in the tropopause region. During a cloud observed on 25 January 2000 (data shown in Figure 3), the background water vapor abundance ranged between 10 and 25 ppm. Under these conditions, a single 100- $\mu\text{m}$  particle, present at a concentration of about  $4 \times 10^{-3} \text{ cm}^{-3}$ , as inferred from the IWC discrepancy, would be able to remove as much as 10 ppm of water as it fell. This is clearly a significant fraction, between 30 and 50%, of the available water.

[36] Some additional corroborating evidence is available from observations made by the NASA Langley Lidar Atmospheric Sensing Experiment (LASE) instrument aboard the DC-8 [Moore *et al.*, 1997]. LASE measures water vapor mixing ratios and aerosol backscatter in both the zenith and nadir directions. We have used these data to estimate the location of the plane with respect to cloud boundaries for each cirrus cloud encounter. These estimates are limited by the lack of data within approximately 1 km of the plane, so it is only possible to separate the particulate water measurements into two categories: upper/middle cloud and middle/lower cloud. In general, when the plane flew in the upper/middle cloud regions there is a smaller difference between the CLH and FSSP ice water content than when data were obtained in the middle/lower cloud regions. While this observation is only empirical, it is consistent with the presence of large particles (outside of the FSSP-300 measurement range), given that the larger particles tend to settle to the lower part of the cloud [Kinne *et al.*, 1997].

[37] This observation can be further substantiated by looking at the relative humidity (RH) of the sampled air in the cloudy regions. We have used the DC-8 operational temperature sensor to define the ambient temperature, and hence, saturation mixing ratio ( $e_s$ ) and the JLH water measurements ( $e$ ) to determine RH ( $e/e_s$ ) with respect to ice. It is estimated that the DC-8 temperature values are good to  $\pm 1$  K. This uncertainty in temperature couples into the RH through the calculation of  $e_s$ ; at temperatures around 200 K, a 1 K temperature error leads to an error in RH of at least  $\pm 15\%$  [Buehler and Courcoux, 2003]. For the cloud periods described in this study, RH was calculated for all time periods when CLH, JLH, and FSSP data were available. These data were then grouped into “saturated” ( $85\% < \text{RH} < 115\%$ ), “supersaturated” ( $\text{RH} \geq 115\%$ ), and “sub-saturated” ( $\text{RH} \leq 85\%$ ) regimes. The differences in IWC determined from the CLH observations and that calculated from FSSP size distributions were grouped together for each of the three RH regimes and averaged.

[38] On all flight dates the CLH/FSSP differences were nearly identical for “saturated” and “supersaturated” cases. On three of the four dates (insufficient data existed for 8 March 2000 to be included in this analysis), however, there were substantially larger differences for the “sub-saturated” case by factors of 50–300% (on 25 January 2000, the sub-saturated case was similar to the others). These differences between the IWC calculated from CLH and from FSSP observations are consistent with expectations about the relationship between RH and particle sizes. Other observations in cirrus have shown that supersaturations and small particles are typically present near the tops of clouds [Ström *et al.*, 2003]. The presence of particles in sub-saturated regimes must indicate large sizes, given that smaller particles evaporate more quickly than larger ones in a nonequilibrium situation. Thus the larger differences between CLH and FSSP IWC values in sub-saturated regions is further evidence that large particles outside the FSSP diameter range are present.

[39] As noted in section 1, several recent studies have demonstrated the presence of nitric acid on or in cirrus cloud particles that are composed primarily of ice. Kondo *et al.* [2003] analyzed particulate reactive nitrogen ( $\text{NO}_y$ ) observations made from the DC-8 during SOLVE. They showed that  $\text{HNO}_3$  coverage on cirrus cloud particles can exceed  $1 \times 10^{14}$  molecules  $\text{cm}^{-2}$  of particle surface at temperatures below 210 K. As cirrus cloud particles sediment, they carry with them  $\text{HNO}_3$ , in varying amounts, ultimately redistributing it to lower altitudes as the particle composition and size adjust to different ambient temperature and trace gas partial pressures. The presence of cirrus cloud particles with diameters as large as 100  $\mu\text{m}$  not only provides considerable additional surface area for adsorption of volatile gases such as  $\text{HNO}_3$ , but, as noted above, faster sedimentation to lower regions of the atmosphere. A similar process was observed during the SOLVE campaign with the sedimentation of very large nitric acid trihydrate (NAT) particles from higher altitudes through the 18–20 km region of the stratosphere [Fahey *et al.*, 2001; Northway *et al.*, 2002].

[40] The presence of cirrus cloud particles that are larger than expected based on temperature also has implications for heterogeneous chemical processes. Typically, the rates of these reactions on solid particles are dependent on particle surface area, which scales with the square of the

radius. Given that the surface area of a 100  $\mu\text{m}$  particle is 100 times greater than that of a 10  $\mu\text{m}$  particle, the presence of just a few large particles can make a substantial difference in the rates of heterogeneous processes. Using the relationship between IWC and surface area density described by *Lawrence and Crutzen* [1998], we estimate, using the CLH IWC, that the clouds encountered during SOLVE have minimum surface areas ranging between 20 and 100  $\mu\text{m}^2 \text{cm}^{-3}$ . How this large surface area density affects heterogeneous rates will depend sensitively on the details of the size distribution; for a fixed IWC, more smaller particles will contribute greater surface area density than a few large ones. Nonetheless, the presence of particles outside the measured size distribution can have a profound impact.

[41] *Lelieveld et al.* [1999] describe the sampling of trace gases such as CO and ethane ( $\text{C}_2\text{H}_6$ ) in the tropopause region, in the vicinity of thin cirrus clouds. They show that heterogeneous production of chlorine atoms from reservoir chlorine species such as HCl and  $\text{ClONO}_2$  is efficient enough with particle surface areas as small as  $1.5 \times 10^3 \mu\text{m}^2 \text{cm}^{-3}$  to cause a noticeable change in the ratio of  $\text{CO}/\text{C}_2\text{H}_6$  because of Cl-induced ethane destruction. These clouds were of comparable number density to those sampled in SOLVE, so we might expect the SOLVE cirrus to have had a detectable effect on trace gas abundances, including chlorine and ozone (B. F. Thornton et al., Mechanism of chlorine activation near the winter Arctic tropopause, manuscript in preparation, 2004). Modeling studies carried out by *Kärcher and Solomon* [1999] also indicate that heterogeneous activation of chlorine is possible on cirrus cloud particles in the tropopause region, although its magnitude is sensitive to parameters such as the relative humidity and particle surface area.

## 6. Summary

[42] We have presented measurements of total water made during the SOLVE campaign using a closed-path tunable diode laser hygrometer (CLH). During cloud-free periods, CLH observations agreed to within 2 ppmv with open-path TDL measurements of water vapor from JPL's JLH instrument. Comparisons of ice water content (IWC) derived from the CLH data with that calculated from size distributions measured by a FSSP, assuming spherical ice particles, revealed considerable differences. The CLH instrument typically reported 15 to 35 ppmv more condensed water than was suggested by the FSSP size distributions during all cirrus cloud encounters.

[43] Since the upper size limit for the FSSP instrument during this campaign was set at 20  $\mu\text{m}$ , we have suggested that larger, and hence undetected, crystals are present in these Arctic cirrus. A simple lognormal extension of the existing size distribution is inadequate to explain the observed IWC. A mass distribution constructed from observations of ice crystals in midlatitude cirrus at temperatures similar to those sampled in the Arctic shows the presence of a distinct mode at diameters between 100 and 150  $\mu\text{m}$ . Including such a mode in the size distribution for the Arctic clouds results in considerably better correspondence with the measured IWC.

[44] This study provides compelling evidence for the existence of large ( $d > 20 \mu\text{m}$ ) particles within Arctic cirrus clouds. Owing to the importance of cirrus clouds both in the global energy balance and in chemical transformations within the reactive nitrogen and halogen families via surficial reactions, these results could be significant on a global scale.

[45] **Acknowledgments.** We are indebted to R. D. May for help with technical issues related to the CLH instrument and to E. S. Whitney for performing laboratory calibrations. We would like to thank M. J. Mahoney, S. Kinne, B. Gandrud, O. B. Toon, and D. Baumgardner for helpful discussions. We appreciate the support of the DC-8 pilots and ground crew during the SOLVE mission. Support for the deployment of the CLH instrument was provided by the NASA AEAP program under the direction of D. L. Anderson.

## References

- Abbatt, J. P. D. (1997), Interaction of  $\text{HNO}_3$  with water-ice surfaces at temperatures of the free troposphere, *Geophys. Res. Lett.*, *24*, 1479.
- Baumgardner, D., J. E. Dye, B. W. Gandrud, and R. G. Knollenberg (1992), Interpretation of measurements made by the forward scattering spectrometer probe (FSSP-300) during the airborne arctic stratospheric expedition, *J. Geophys. Res.*, *97*, 8035.
- Belyaev, S. P., and L. M. Levin (1972), Investigation of aerosol aspiration by photographing particle tracks under flash illumination, *Aerosol Sci.*, *3*, 127.
- Booker, D. R., and P. G. Stickel (1982), High altitude tropical cirrus cloud observations, Preprints, paper presented at Conference on Cloud Physics, Am. Meteorol. Soc., Chicago, Ill.
- Borrmann, S., S. Solomon, J. E. Dye, and B. Luo (1996), The potential of cirrus clouds for heterogeneous chlorine activation, *Geophys. Res. Lett.*, *23*, 2133.
- Bregman, B., P.-H. Wang, and J. Lelieveld (2002), Chemical ozone loss in the tropopause region on subvisible ice clouds, calculated with a chemistry-transport model, *J. Geophys. Res.*, *107*(D3), 4032, doi:10.1029/2001JD000761.
- Buehler, S. A., and N. Courcoux (2003), The impact of temperature errors on perceived humidity supersaturation, *Geophys. Res. Lett.*, *30*(14), 1759, doi:10.1029/2003GL017691.
- Dowling, D. R., and L. F. Radke (1990), A summary of the physical properties of cirrus clouds, *J. App. Meteorol.*, *29*, 970.
- Fahey, D. W., K. K. Kelly, G. V. Ferry, L. R. Poole, J. C. Wilson, D. M. Murphy, M. Loewenstein, and K. R. Chan (1989), In situ measurements of total reactive nitrogen, total water, and aerosol in a polar stratospheric cloud in the Antarctic, *J. Geophys. Res.*, *94*, 11,299.
- Fahey, D. W., et al. (2001), The detection of large  $\text{HNO}_3$ -containing particles in the winter Arctic stratosphere, *Science*, *291*, 1026.
- Fan, S. M., et al. (1994), Origin of tropospheric  $\text{NO}_x$  over subarctic eastern Canada in summer, *J. Geophys. Res.*, *99*, 16,867.
- Feigl, C., H. Schlager, H. Ziereis, J. Curtius, F. Arnold, and C. Schiller (1999), Observation of  $\text{NO}_x$  uptake by particles in the Arctic tropopause region at low temperatures, *Geophys. Res. Lett.*, *26*, 2215.
- Field, P. R., R. Wood, P. R. A. Brown, P. H. Kaye, E. Hirst, R. Greenaway, and J. A. Smith (2003), Ice particle interarrival times measured with a fast FSSP, *J. Atmos. Oceanic Technol.*, *20*, 249.
- Gardiner, B. A., and J. Hallett (1985), Degradation of in-cloud forward scattering spectrometer probe measurements in the presence of ice particles, *J. Atmos. Oceanic Technol.*, *2*, 171.
- Goodman, J., O. B. Toon, R. F. Pueschel, K. G. Snetsinger, and S. Verma (1989), Antarctic stratospheric ice crystals, *J. Geophys. Res.*, *94*, 16,499.
- Hervig, M., and M. McHugh (2002), Tropical nitric acid clouds, *Geophys. Res. Lett.*, *29*(7), 1125, doi:10.1029/2001GL014271.
- Heymsfield, A. J. (1986), Ice particles observed in a cirriform cloud at  $-83^\circ\text{C}$  and implications for polar stratospheric clouds, *J. Atmos. Sci.*, *43*, 851.
- Heymsfield, A. J., and L. J. Jahnsen (1974), Microstructure of tropopause cirrus layers, paper presented at Sixth Conference on Aerospace and Aeronautical Meteorology, Am. Meteorol. Soc., El Paso, Tex.
- Heymsfield, A. J., and C. M. R. Platt (1984), A parameterization of the particle-size spectrum of ice clouds in terms of the ambient-temperature and the ice water-content, *J. Atmos. Sci.*, *41*, 846.
- Hynes, R. G., M. A. Fernandez, and R. A. Cox (2002), Uptake of  $\text{HNO}_3$  on water-ice and coadsorption of  $\text{HNO}_3$  and HCl in the temperature range 210–235 K, *J. Geophys. Res.*, *107*(D24), 4797, doi:10.1029/2001JD001557.
- Intergovernmental Panel on Climate Change (IPCC) (2001), *Climate Change 2001: The Scientific Basis*, Cambridge Univ. Press, New York.



- Jensen, E., D. Starr, and O. Toon (2004), Mission investigates tropical cirrus clouds, *Eos AGU Trans.*, 85 (5), 45, 50.
- Kärcher, B., and S. Solomon (1999), On the composition and optical extinction of particles in the tropopause region, *J. Geophys. Res.*, 104, 27,441.
- Kinne, S., and K. N. Liou (1989), The effects of non-sphericity and size distribution of ice-crystals on the radiative properties of ice-clouds, *Atmos. Res.*, 24, 273.
- Kinne, S., et al. (1997), Cirrus cloud radiative and microphysical properties from ground observations and in situ measurements during FIRE 1991 and their application to exhibit problems in cirrus solar radiative transfer modeling, *J. Atmos. Sci.*, 54, 2320.
- Kondo, Y., et al. (2003), Uptake of reactive nitrogen on cirrus cloud particles in the upper troposphere and lowermost stratosphere, *Geophys. Res. Lett.*, 30(4), 1154, doi:10.1029/2002GL016539.
- Lawrence, M. G., and P. J. Crutzen (1998), The impact of particle gravitational settling on soluble trace gas distributions, *Tellus, Ser. B*, 50, 263.
- Lelieveld, J., A. Bregman, H. A. Scheeren, J. Ström, K. S. Carslaw, H. Fischer, P. C. Siegmund, and F. Arnold (1999), Chlorine activation and ozone destruction in the northern lowermost stratosphere, *J. Geophys. Res.*, 104, 8201.
- Logan, J. A., et al. (1999), Trends in the vertical distribution of ozone: A comparison of two analyses of ozonesonde data, *J. Geophys. Res.*, 104, 26,373.
- Lohmann, U., and E. Roeckner (1995), Influence of cirrus cloud radiative forcing on climate and climate sensitivity in a general circulation model, *J. Geophys. Res.*, 100, 16,305.
- May, R. D. (1998), Open-path, near-infrared tunable diode laser spectrometer for atmospheric measurements of H<sub>2</sub>O, *J. Geophys. Res.*, 103, 19,161.
- McFarquhar, G. M., A. J. Heymsfield, J. Spinhirne, and B. Hart (2000), Thin and subvisual tropopause tropical cirrus: Observations and radiative impacts, *J. Atmos. Sci.*, 57, 1841.
- Meilinger, S. K., et al. (1999), HNO<sub>3</sub> partitioning in cirrus clouds, *Geophys. Res. Lett.*, 26, 2207.
- Miloshevich, L. M., and A. J. Heymsfield (1997), A balloon-borne continuous cloud particle replicator for measuring vertical profiles of cloud microphysical properties: Instrument design, performance, and collection efficiency analysis, *J. Atmos. Oceanic Technol.*, 14, 753.
- Moore, A. S., et al. (1997), Development of the Lidar Atmospheric Sensing Experiment (LASE), an advanced airborne DIAL instrument, in *Advances in Atmospheric Remote Sensing with Lidar*, edited by A. Ansmann et al., pp. 281–288, Springer-Verlag, New York.
- Newman, P. A., et al. (2002), An overview of the SOLVE/THESEO 2000 campaign, *J. Geophys. Res.*, 107(D20), 8259, doi:10.1029/2001JD001303.
- Northway, M. J., et al. (2002), An analysis of large HNO<sub>3</sub>-containing particles sampled in the Arctic stratosphere during the winter of 1999/2000, *J. Geophys. Res.*, 107(D20), 8298, doi:10.1029/2001JD001079.
- Peter, T., et al. (2003), Ultrathin Tropical Tropopause Clouds (UTTCs): I. Cloud morphology and occurrence, *Atmos. Chem. Phys.*, 3, 1083.
- Roe, J. M., and W. H. Jasperson (1980), A new tropopause definition from simultaneous ozone-temperature profiles, *Tech. Rep. AFGL-TR-80-0289*, Air Force Geophys. Lab., Hanscom Air Force Base, Mass.
- Schiller, C., et al. (1999), Ice particle formation and sedimentation in the tropopause region: A case study based on in situ measurements of total water during POLSTAR 1997, *Geophys. Res. Lett.*, 26, 2219.
- Schlichting, H. (1979), *Boundary Layer Theory*, rev. ed., McGraw-Hill, New York.
- Singh, H. B., et al. (1994), Summertime distribution of PAN and other reactive nitrogen species in the northern high-latitude atmosphere of eastern Canada, *J. Geophys. Res.*, 99, 1821.
- Smith, J. B., E. J. Hints, N. T. Allen, R. M. Stimpfle, and J. G. Anderson (2001), Mechanisms for midlatitude ozone loss: Heterogeneous chemistry in the lowermost stratosphere?, *J. Geophys. Res.*, 106, 1297.
- Ström, J., and J. Heintzenberg (1994), Water-vapor, condensed water, and crystal concentration in orographically influenced cirrus clouds, *J. Atmos. Sci.*, 51, 2368.
- Ström, J., et al. (2003), Cirrus cloud occurrence as function of ambient relative humidity: A comparison of observations from the Southern and Northern Hemisphere midlatitudes obtained during the INCA experiment, *Atmos. Chem. Phys. Discuss.*, 3, 3301.
- Sun, Z., and L. Rikus (1999), Parameterization of effective sizes of cirrus-cloud particles and its verification against observations, *Q. J. R. Meteorol. Soc.*, 125, 3037.
- Thomas, A., et al. (2002), In situ measurements of background aerosol and subvisible cirrus in the tropical tropopause region, *J. Geophys. Res.*, 107(D24), 4763, doi:10.1029/2001JD001385.
- Thornton, B. F., D. W. Toohey, L. M. Avallone, H. Harder, M. Martinez, J. B. Simpas, W. H. Brune, and M. A. Avery (2003), In situ observations of ClO near the winter polar tropopause, *J. Geophys. Res.*, 108(D8), 8333, doi:10.1029/2002JD002839.
- Weinheimer, A. J., T. L. Campos, J. G. Walega, F. E. Grahek, B. A. Ridley, D. Baumgardner, C. H. Twohy, B. Gandrud, and E. J. Jensen (1998), Uptake of NO<sub>y</sub> on wave-cloud ice particles, *Geophys. Res. Lett.*, 25, 1725.
- Wylie, D. P., and W. P. Menzel (1999), Eight years of high cloud statistics using HIRS, *J. Clim.*, 12, 170.
- Wylie, D. P., W. P. Menzel, H. M. Woolf, and K. I. Strabala (1994), 4 years of global cirrus cloud statistics using HIRS, *J. Clim.*, 7, 1972.
- Zondlo, M. A., S. B. Barone, and M. A. Tolbert (1997), Uptake of HNO<sub>3</sub> on ice under upper tropospheric conditions, *Geophys. Res. Lett.*, 24, 1391.
- Zondlo, M. A., P. K. Hudson, A. J. Prenni, and M. A. Tolbert (2000), Chemistry and microphysics of polar stratospheric clouds and cirrus clouds, *Ann. Rev. Phys. Chem.*, 51, 473.

B. E. Anderson, NASA Langley Research Center, Mail Stop 483, Hampton, VA 23681-2199, USA.

L. M. Avallone, Laboratory for Atmospheric and Space Physics, University of Colorado, 590 UCB, Boulder, CO 80309-0590, USA. (avallone@lasp.colorado.edu)

A. G. Hallar, NASA Ames Research Center, Mail Stop 245-4, Moffett Field, CA 94035-1000, USA.

R. L. Herman, Jet Propulsion Laboratory, California Institute of Technology, 4800 Oak Grove Drive, Pasadena, CA 91109-8099, USA.

A. J. Heymsfield, National Center for Atmospheric Research, P. O. Box 3000, Boulder, CO 80307-3000, USA.